

JOINT DEMOSAICING AND DENOISING WITH DOUBLE DEEP IMAGE PRIORS

Taihui Li^{1*} Anish Lahiri² Yutong Dai² Owen Mayer²

¹ Computer Science and Engineering, University of Minnesota, Minneapolis, USA

² Sony Corporation of America, R&D US Laboratory, San Jose, USA

ABSTRACT

Demosaicing and denoising of RAW images are crucial steps in the processing pipeline of modern digital cameras. As only a third of the color information required to produce a digital image is captured by the camera sensor, the process of demosaicing is inherently ill-posed. The presence of noise further exacerbates this problem. Performing these two steps sequentially may distort the content of the captured RAW images and accumulate errors from one step to another. Recent deep neural-network-based approaches have shown the effectiveness of joint demosaicing and denoising to mitigate such challenges. However, these methods typically require a large number of training samples and do not generalize well to different types and intensities of noise. In this paper, we propose a novel joint demosaicing and denoising method, dubbed JDD-DoubleDIP, which operates directly on a single RAW image without requiring any training data. We validate the effectiveness of our method on two popular datasets—Kodak and McMaster—with various noises and noise intensities. The experimental results show that our method consistently outperforms other compared methods in terms of PSNR, SSIM, and qualitative visual perception.

Index Terms— Image Signal Processing, Deep Image Prior, RAW Images, Demosaicing, Denoising

1. INTRODUCTION

A RAW image (a.k.a. mosaic image) is sensor data directly captured by digital cameras. In RAW images, only a third of the color information required to produce a high-quality full-color RGB image is available. Hence, demosaicing is necessary to interpolate the missing color components. However, this is inherently an ill-posed problem [1, 2] and the presence of noise in RAW images due to various factors (e.g., Poisson noise due to lighting conditions, Gaussian noise from electronics, etc.) further exacerbates this problem [3]. Traditionally, demosaicing and denoising are handled sequentially in the camera processing pipeline, but this may lead to content distortion in images and the accumulation of errors from one processing step to another. Furthermore, determining the optimal processing order also becomes a challenge [4, 5].

In contrast, adopting a joint demosaicing and denoising (JDD) strategy can naturally overcome the aforementioned challenges [6, 1]. Classical methods for JDD include the specialized design of filters with constraints [6] and the use of certain heuristics such as total variation minimization [7], self-similarity [8], learned nonparametric random fields [9], and sequential energy minimization [10]. Recently, with the resurgence of deep neural networks (DNNs), several studies [1, 11, 2, 12] have shown the benefits of DNN-based JDD over traditional methods. One main stream among these methods is data-driven JDD. Gharbi et al. [1] cast JDD as a supervised

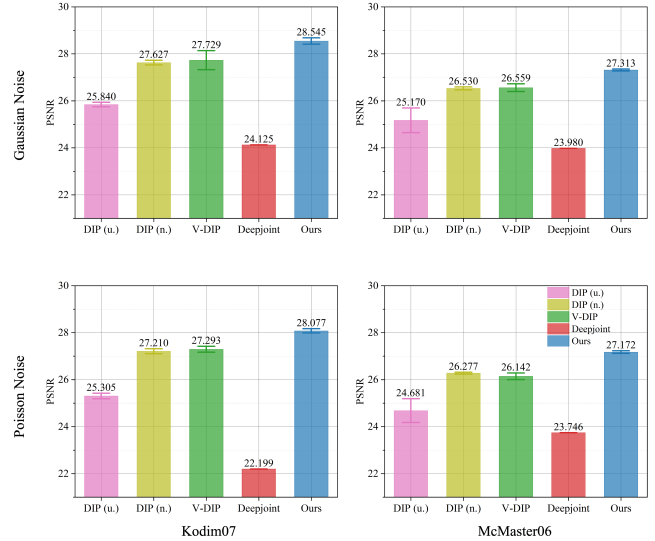


Fig. 1. The PSNR comparisons of demosaicing and denoising on RAW images—Kodim07 (first column) and McMaster06 (second column)—with Gaussian noise $\sigma = 30$ (first row) and Poisson noise $\lambda = 25$ (second row). We provide comprehensive comparisons in Table 1 and Table 2.

learning problem and use a convolutional neural network to directly learn a mapping between noisy RAW images and full-color RGB images. Ehret et al. [11] propose a mosaic-to-mosaic training strategy that learns demosaicing and denoising on RAW images only, without full-color ground-truth RGB images. Liu et al. [2] design an additional branch to estimate the green channel and then use the estimated green channel as a guide to recover all missing values. Though these methods have significantly improved the demosaicing and denoising performance, they require massive training data to learn the models well. It is not only expensive to acquire these data sets, but there are no ground-truth data in practice. Worse, once a DNN model has been trained on a particular noise and noise intensity, it does not generalize well to other noise and noise intensities.

This motivates the need for developing single-instance JDD methods. The recent deep image prior (DIP) method [13] demonstrates that the neural network itself can serve as an implicit prior for natural images to solve image restoration problems by fitting a single noisy observation. Although DIP has garnered growing interest recently, its application in RAW image demosaicing remains relatively scarce. Park et al. [12] for the first time present a DIP-based approach (V-DIP) for RAW image demosaicing and denoising, obviating the need for training data. However, V-DIP has an additional optimization objective to update targets and formulates the problem as image inpainting without explicitly considering denoising.

To address the limitations of V-DIP, we propose a dual-branch

*Work performed while at Sony Corporation of America.

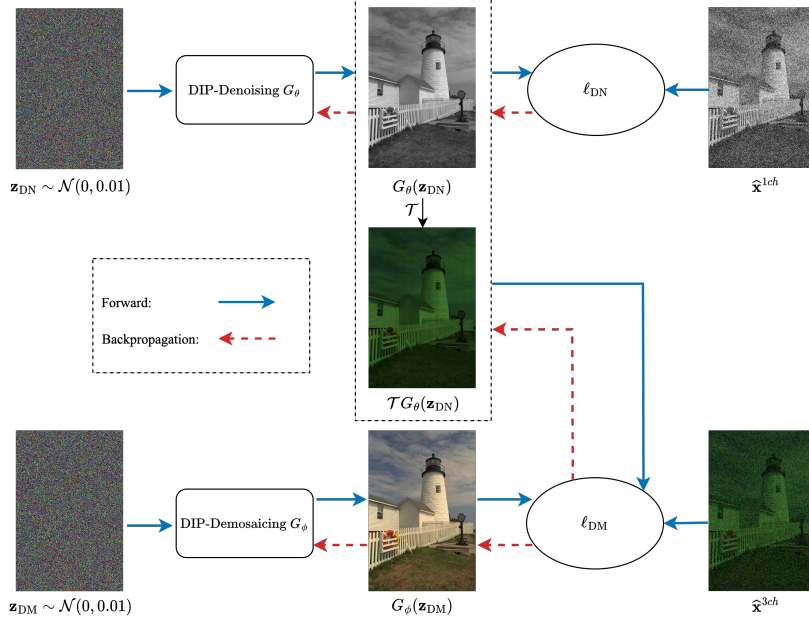


Fig. 2. Framework of JDD-DoubleDIP, consisting of a *DIP-Denoising* G_θ and a *DIP-Demaicing* G_ϕ . G_θ is used to denoise the given noisy RAW image and provide “clean” guidance to G_ϕ ; while G_ϕ attempts to recover the desired high-quality full-color RGB image based on 1) the given noisy RAW image $\hat{\mathbf{x}}^{3ch}$ and 2) the denoised output of G_θ . We join these two branches by combining their respective losses $\ell_{\text{JDD-DoubleDIP}} = \sqrt{\ell_{\text{DN}}} + \sqrt{\ell_{\text{DM}}}$ and train them simultaneously. By doing so, these two branches collaborate with each other, yielding better demosaicing and denoising results.

model, dubbed *JDD-DoubleDIP*, which utilizes information from a denoising DIP branch to guide the joint demosaicing and denoising objective. To do this, we first adopt a DIP dedicated to account for noise removal (*denoising*). Then, we employ a second DIP which jointly performs denoising and missing-value interpolation (*demosaicing*), and is guided by the output from the denoising DIP. We join these two DIPs by amalgamating their respective loss functions into a single optimization objective and update their parameters simultaneously. By doing so, we have not only explicitly induced denoising guidance information into the model, but we also enabled these two DIPs to collaborate with each other for better performance. Fig. 1 shows the superiority of our model over other models.

2. OUR METHOD

2.1. Background: Deep Image Prior

Given a single noisy observation \mathbf{y} , deep image prior (DIP) [13] uses a structured deep neural network $G_\theta(\cdot)$ parameterized by θ to fit this noisy observation and restore its corresponding clean image \mathbf{x} . Specifically, DIP solves the following optimization problem:

$$\min_{\theta} \ell(\mathbf{y}, f \circ G_\theta(\mathbf{z})) \quad (1)$$

where \circ denotes function composition, f represents the forward measurement operator (e.g., f is an identity operator for image denoising), \mathbf{z} is a random input seed sampling from a uniform distribution, and ℓ is a loss function (e.g., mean squared error). After obtaining the optimal solution θ^* of Eq. (1), the clean image \mathbf{x} could be easily restored with a forward pass $G_{\theta^*}(\mathbf{z})$. Despite the fact that DIP is learned without any training dataset, it has shown tremendous promise in a variety of tasks ranging from classical image restoration [13, 14, 15], to advanced computational imaging problems [16, 17, 18], and even beyond (e.g., time series [19]).

2.2. Problem Formulation

We represent the clean RAW image as $\mathbf{x}^{1ch} \in \mathbb{R}^{H \times W}$, noise as $\mathbf{n} \in \mathbb{R}^{H \times W}$, and the noisy RAW image as $\hat{\mathbf{x}}^{1ch} = \mathbf{x}^{1ch} + \mathbf{n}$, where H and W are the height and width of the image. We further define a mask $\mathbf{m} \in \mathbb{R}^{H \times W \times 3}$, where each spatial location has 1 in the channel corresponding to the color acquired at that position in the RGGGB Bayer pattern, 0 in other channels. We also introduce an operation \mathcal{T} , which maps the single-channel RAW data into a full-color image, where the non-Bayer components are 0 (representing the missing pixels) and the originally sampled RAW data placed at the respective Bayer location and channels.

The goal of JDD is to reconstruct a high-quality full-color RGB image $\mathbf{x}^{3ch} \in \mathbb{R}^{H \times W \times 3}$ from a single noisy observation $\hat{\mathbf{x}}^{3ch} = \mathcal{T}\hat{\mathbf{x}}^{1ch}$. To do so, we need to fill in the missing pixels in the RAW image $\hat{\mathbf{x}}^{3ch}$ (*demosaicing*), as well as to remove noisy components \mathbf{n} (*denoising*). In a manner similar to V-DIP [12], we also formulate the demosaicing procedure as an image-inpainting problem, since both attempt to reconstruct the absent pixels.

2.3. Double DIPs for Joint Demosaicing and Denoising

DIP can restore high-quality images for inpainting when the observation is clean [13, 14], however, its performance deteriorates dramatically if additional noise is present [20]. Thus, we posit that conceptualizing the demosaicing procedure as an inpainting task and employing a DIP to directly restore absent values, without meticulous consideration of noise removal, may lead to suboptimal solutions.

To overcome this limitation, we introduce a novel dual-branch model for demosaicing (DM) and denoising (DN), dubbed *JDD-DoubleDIP*, which consists of two DIPs (see Fig. 2): *DIP-Denoising* G_θ , parameterized by θ and *DIP-Demaicing*¹ G_ϕ , parameterized

¹We refer to this branch as DIP-Demaicing simply to differentiate it from the denoising branch, but we note that it actually performs *joint* demo-

Table 1. The quantitative results of demosaicing and denoising of RAW images with Gaussian noise. **Deepjoint**: we use the maximum noise intensity of the pretrained model as input. **Deepjoint***: we use the exact noise intensity of the noisy RAW image as input. **Ours⁺**: we smooth the output of our model by using running average: $\hat{x}_{\text{smooth}}^{3ch} = 0.99 * x_{\text{smooth}}^{3ch} + 0.01 * G_{\phi}(z_{\text{DM}})$.

Dataset	Method	PSNR \uparrow					SSIM \uparrow				
		$\sigma=10$	$\sigma=20$	$\sigma=30$	$\sigma=50$	$\sigma=70$	$\sigma=10$	$\sigma=20$	$\sigma=30$	$\sigma=50$	$\sigma=70$
Kodak	DIP (u.)	29.383 (0.038)	26.521 (0.021)	24.786 (0.017)	22.707 (0.021)	21.369 (0.014)	0.811 (0.0012)	0.682 (0.0010)	0.595 (0.0021)	0.494 (0.0028)	0.443 (0.0033)
	DIP (n.)	30.061 (0.028)	27.594 (0.071)	26.104 (0.015)	24.132 (0.009)	22.594 (0.014)	0.840 (0.0009)	0.748 (0.0030)	0.684 (0.0010)	0.589 (0.0015)	0.516 (0.0009)
	V-DIP	29.664 (0.154)	27.393 (0.037)	25.872 (0.022)	23.792 (0.027)	22.269 (0.043)	0.834 (0.0053)	0.759 (0.0019)	0.703 (0.0005)	0.614 (0.0014)	0.544 (0.0013)
	Deepjoint	30.040 (N/A)	29.998 (N/A)	23.796 (N/A)	17.494 (N/A)	14.558 (N/A)	0.792 (N/A)	0.818 (N/A)	0.482 (N/A)	0.231 (N/A)	0.144 (N/A)
	Deepjoint*	33.222 (N/A)	29.995 (N/A)	27.828 (N/A)	24.068 (N/A)	19.665 (N/A)	0.902 (N/A)	0.818 (N/A)	0.717 (N/A)	0.447 (N/A)	0.165 (N/A)
	Ours	30.758 (0.046)	28.493 (0.055)	26.987 (0.034)	24.776 (0.016)	23.043 (0.026)	0.865 (0.0014)	0.788 (0.0009)	0.730 (0.0008)	0.648 (0.0018)	0.593 (0.0014)
	Ours ⁺	31.149 (0.048)	28.919 (0.062)	27.382 (0.037)	25.014 (0.019)	23.119 (0.030)	0.874 (0.0018)	0.803 (0.0010)	0.746 (0.0002)	0.662 (0.0020)	0.603 (0.0020)
McMaster	DIP (u.)	29.921 (0.029)	26.703 (0.031)	24.760 (0.036)	22.384 (0.060)	20.354 (0.013)	0.828 (0.0008)	0.701 (0.0013)	0.610 (0.0022)	0.510 (0.0028)	0.418 (0.0039)
	DIP (n.)	30.843 (0.016)	28.065 (0.026)	26.155 (0.005)	23.450 (0.008)	21.391 (0.013)	0.859 (0.0001)	0.768 (0.0008)	0.690 (0.0007)	0.568 (0.0009)	0.481 (0.0018)
	V-DIP	30.887 (0.036)	27.902 (0.036)	25.844 (0.039)	23.146 (0.056)	21.192 (0.041)	0.863 (0.0007)	0.777 (0.0007)	0.703 (0.0011)	0.590 (0.0022)	0.508 (0.0019)
	Deepjoint	30.497 (N/A)	30.146 (N/A)	24.083 (N/A)	17.987 (N/A)	14.890 (N/A)	0.835 (N/A)	0.823 (N/A)	0.510 (N/A)	0.257 (N/A)	0.164 (N/A)
	Deepjoint*	33.142 (N/A)	30.140 (N/A)	27.953 (N/A)	24.012 (N/A)	19.495 (N/A)	0.903 (N/A)	0.834 (N/A)	0.744 (N/A)	0.486 (N/A)	0.207 (N/A)
	Ours	31.544 (0.060)	28.739 (0.028)	26.880 (0.013)	24.075 (0.038)	21.906 (0.020)	0.876 (0.0009)	0.793 (0.0011)	0.726 (0.0013)	0.623 (0.0020)	0.552 (0.0012)
	Ours ⁺	32.043 (0.056)	29.198 (0.024)	27.228 (0.015)	24.225 (0.028)	21.906 (0.022)	0.884 (0.0007)	0.804 (0.0008)	0.738 (0.0012)	0.634 (0.0017)	0.561 (0.0018)

by ϕ . Specifically, *DIP-Denoising* G_{θ} is dedicated to remove the noisy components in the given noisy single-channel RAW image \hat{x}^{1ch} . Its loss function thus can be formulated as Eq. (2):

$$\ell_{\text{DN}} = \ell(\hat{x}^{1ch}, G_{\theta}(z_{\text{DN}})) \quad (2)$$

where z_{DN} is a random seed sampled from a normal distribution and ℓ is a distance measurement function (e.g., mean squared error).

DIP-Demosaicing G_{ϕ} , on the other hand, is tailored to generate the desired high-quality full-color RGB image x^{3ch} . Unlike V-DIP [12], which reconstructs x^{3ch} only based on the given noisy RAW image \hat{x}^{3ch} , our *DIP-Demosaicing* accomplishes this goal by making use of two sources of information—the given noisy RAW image \hat{x}^{3ch} and the reconstructed result of the *DIP-Denoising*. Therefore, the loss function of *DIP-Demosaicing* consists of two components, as shown in Eq. (3):

$$\begin{aligned} \ell_{\text{DM}} = & \ell(TG_{\theta}(z_{\text{DN}}) \odot m, G_{\phi}(z_{\text{DM}}) \odot m) \\ & + \alpha \ell(\hat{x}^{3ch} \odot m, G_{\phi}(z_{\text{DM}}) \odot m) \end{aligned} \quad (3)$$

where the first term simulates the procedure of using *DIP-Demosaicing* to demosaic a denoised (“clean”) RAW image while the second term accounts for the original noisy RAW image demosaicing. We use α to weight the second loss term. Similarly, the input z_{DM} is sampled from a normal distribution and ℓ is the mean squared error.

Finally, we couple *DIP-Denoising* and *DIP-Demosaicing* together with a joint loss function, as shown in Eq. (4):

$$\ell_{\text{JDD-DoubleDIP}} = \sqrt{\ell_{\text{DN}}} + \sqrt{\ell_{\text{DM}}} \quad (4)$$

We use the square root of ℓ_{DN} and ℓ_{DM} to further suppress the effects of noise. We hypothesize that *DIP-Denoising* offers a form of “clean” guidance to *DIP-Demosaicing*, enabling the latter to demosaic a “clean” RAW image; conversely, *DIP-Demosaicing* serves as a mechanism for providing “feedback” to *DIP-Denoising*, facilitating the removal of noisy components. Therefore, by training these two neural networks jointly, we expect to see improved performance of demosaicing and denoising.

saicing and denoising as its reconstruction is based on both the given noisy RAW image and the denoised output of *DIP-Denoising* branch.

3. EXPERIMENTS

3.1. Experimental Settings

We modify the original DIP [13] architecture slightly for implementing *DIP-Denoising* and *DIP-Demosaicing*: 1) the input seed z_{DN} and z_{DM} are sampled from a normal distribution $\mathcal{N}(0, 0.01)$; 2) the output of *DIP-Denoising* is a single-channel image while the output of *DIP-Demosaicing* is a three-channel image. To verify the effectiveness of our method, we conduct experiments on two popular image datasets—Kodak [21] and McMaster [22]. We also experiment with two common sensor noises—Gaussian noise and Poisson noise—on different noise intensities, ranging from benign to severe scenarios. We compare our method with three single-instance methods—DIP (u.), DIP (n.) [13], V-DIP [12]; as well as one data-driven method—Deepjoint [1]. DIP (u.) indicates that the input z is sampled from a uniform distribution $\mathcal{U}(0, 0.1)$, while in DIP (n.) the input z is sampled from a normal distribution $\mathcal{N}(0, 0.01)$. For the implementation of V-DIP, we adhere to its original paper [12]. For Deepjoint, we employ its official pretrained model which was trained on Gaussian noise intensities $\sigma \in [0, 20]$. For our own model, we fix hyperparameters for all experiments: we set α to 0.1, the learning rate of *DIP-Denoising* to 5×10^{-3} , the learning rate of *DIP-Demosaicing* to 5×10^{-2} , and we use Adam [23] as our optimizer. We adopt PSNR and SSIM as our performance metrics. To ensure the consistency of our observations, we repeat experiments for 5 rounds and then report their mean and standard deviation.

3.2. RAW Images with Gaussian Noise

Here, we first experiment with RAW images corrupted by Gaussian noise. We simulate a noisy RAW image $\hat{x} = x + n$ where $n = \mathcal{N}(0, \sigma)$. σ is varied within $\{10, 20, 30, 50, 70\}$ to account for practical scenarios with different severity.

Table 1 shows the quantitative comparisons. One can observe that: 1) our method consistently outperforms other single-instance methods—DIP (u.), DIP (n.), and V-DIP—on both datasets and across all noise intensities; 2) compared with the data-driven method—Deepjoint² and Deepjoint*³, when the noise intensity is

²Deepjoint: input the maximum noise intensity of the pretrained model.

³Deepjoint*: input the exact noise intensity of the noisy RAW image.

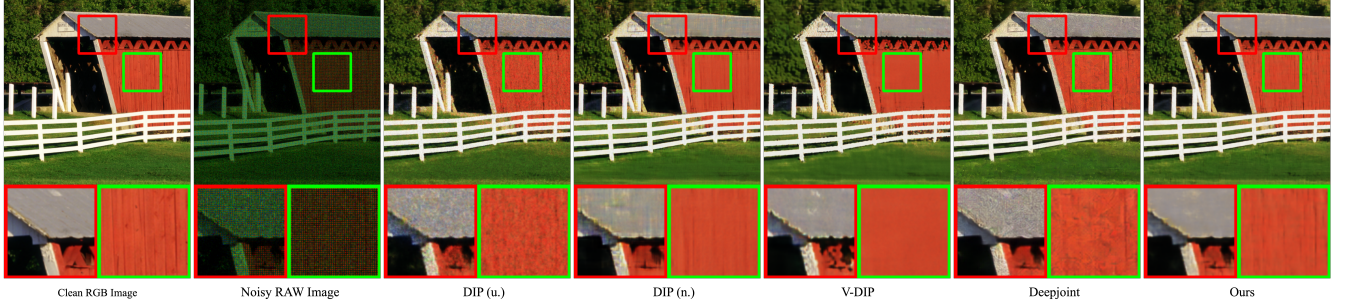


Fig. 3. The visual comparisons of demosaicing and denoising on the RAW image (McMaster18) with Poisson noise ($\lambda = 45$).

Table 2. The quantitative results of demosaicing and denoising of RAW images with Poisson noise. **Deepjoint**: we use the maximum noise intensity of the pretrained model as input. **Ours⁺**: we smooth the output of our model by using running average: $\mathbf{x}_{\text{smooth}}^{3ch} = 0.99 * \mathbf{x}_{\text{smooth}}^{3ch} + 0.01 * G_{\phi}(z_{DM})$.

Dataset	Method	PSNR \uparrow					SSIM \uparrow				
		$\lambda=65$	$\lambda=45$	$\lambda=25$	$\lambda=15$	$\lambda=5$	$\lambda=65$	$\lambda=45$	$\lambda=25$	$\lambda=15$	$\lambda=5$
Kodak	DIP (u.)	26.184 (0.018)	25.429 (0.024)	24.181 (0.023)	23.175 (0.025)	21.069 (0.031)	0.675 (0.0013)	0.637 (0.0015)	0.5766 (0.0011)	0.5301 (0.0018)	0.4506 (0.0028)
	DIP (n.)	27.349 (0.029)	26.662 (0.038)	25.537 (0.016)	24.584 (0.021)	22.297 (0.016)	0.745 (0.0005)	0.716 (0.0010)	0.668 (0.0005)	0.625 (0.0014)	0.519 (0.0008)
	V-DIP	27.131 (0.043)	26.382 (0.053)	25.253 (0.026)	24.174 (0.039)	21.910 (0.023)	0.756 (0.0011)	0.730 (0.0018)	0.687 (0.0002)	0.645 (0.0021)	0.547 (0.0017)
	Deepjoint	28.883 (N/A)	26.850 (N/A)	22.504 (N/A)	19.366 (N/A)	14.728 (N/A)	0.770 (N/A)	0.682 (N/A)	0.487 (N/A)	0.347 (N/A)	0.168 (N/A)
	Ours	28.116 (0.029)	27.436 (0.036)	26.257 (0.041)	25.248 (0.029)	22.750 (0.018)	0.780 (0.0015)	0.754 (0.0008)	0.711 (0.0009)	0.676 (0.0009)	0.593 (0.0018)
	Ours ⁺	28.515 (0.040)	27.820 (0.035)	26.593 (0.036)	25.536 (0.028)	22.844 (0.020)	0.794 (0.0009)	0.769 (0.0005)	0.726 (0.0007)	0.690 (0.0013)	0.602 (0.0012)
McMaster	DIP (u.)	26.610 (0.015)	25.774 (0.040)	24.431 (0.041)	23.412 (0.040)	21.242 (0.028)	0.722 (0.0012)	0.686 (0.0031)	0.627 (0.0028)	0.583 (0.0023)	0.501 (0.0046)
	DIP (n.)	28.074 (0.031)	27.311 (0.024)	26.064 (0.018)	24.940 (0.008)	22.329 (0.011)	0.791 (0.0007)	0.766 (0.0009)	0.720 (0.0012)	0.676 (0.0009)	0.570 (0.0009)
	V-DIP	27.908 (0.040)	26.990 (0.028)	25.664 (0.053)	24.535 (0.009)	22.004 (0.015)	0.801 (0.0012)	0.776 (0.0002)	0.733 (0.0017)	0.692 (0.0009)	0.594 (0.0019)
	Deepjoint	29.149 (N/A)	27.210 (N/A)	23.472 (N/A)	20.590 (N/A)	15.748 (N/A)	0.788 (N/A)	0.715 (N/A)	0.595 (N/A)	0.497 (N/A)	0.299 (N/A)
	Ours	28.805 (0.017)	28.056 (0.022)	26.836 (0.023)	25.698 (0.045)	23.029 (0.031)	0.813 (0.0014)	0.792 (0.0010)	0.753 (0.0012)	0.717 (0.0019)	0.632 (0.0037)
	Ours ⁺	29.286 (0.015)	28.510 (0.019)	27.222 (0.017)	26.019 (0.040)	23.123 (0.036)	0.825 (0.0014)	0.804 (0.0010)	0.766 (0.0013)	0.730 (0.0021)	0.641 (0.0030)

in the distribution of the pretrained model (e.g., $\sigma \in \{10, 20\}$), Deepjoint performs slightly better than our method and Deepjoint* further improves the performance of Deepjoint; while when the test noise intensity is out of the distribution of the pretrained model (e.g., $\sigma \in \{30, 50, 70\}$), the superiority of our approach becomes apparent, even compared with the Deepjoint* setting, thereby validating the distribution shift issue of data-driven methods; 3) applying a running average smoothing on the outputs of our method, which is indicated as Ours⁺, further improves the performance.

Table 3. The comparison of demosaicing and denoising of JDD-DoubleDIP and Over-Parameterization.

Method	Gaussian Noise		Poisson Noise	
	PSNR \uparrow	SSIM \uparrow	PSNR \uparrow	SSIM \uparrow
DM-DM	26.226 (0.246)	0.711 (0.0146)	26.128 (0.199)	0.737 (0.0112)
Ours	26.880 (0.013)	0.726 (0.0013)	26.836 (0.023)	0.753 (0.0012)

3.3. RAW Images with Poisson Noise

Now, we test our method on RAW images with Poisson noise, which is another dominant noise in camera sensors, especially in scenarios with low-light conditions. We simulate the pixel-wise independent Poisson noise as follows: for each pixel $x \in [0, 1]$, the noisy pixel is Poisson distributed with rate λx and we test different intensities of noise by varying $\lambda \in \{65, 45, 25, 15, 5\}$. We report the experimental results in Table 2, which is consistent with our observations in Section 3.2, reassuring the effectiveness of our method.

We also depict a visual comparison in Fig. 3. It is evident that the reconstructions by other methods introduce some artifacts (e.g., residual noise and distortion artifacts), while our reconstruction pre-

serves more texture details and is more perceptually pleasing, reinforcing the benefits of our method.

3.4. JDD-DoubleDIP vs. Over-Parameterization

To verify that the benefits of our method are not a consequence of over-parameterization owing to the use of two DIPs in conjunction, we design a counterpart for our method named *DM-DM* in which we replace *DIP-Denoising* with another *DIP-Demosaicing*, resulting in a network parameterized similarly to ours. For simplicity, here we only experiment with McMaster on Gaussian noise ($\sigma = 30$) and Poisson noise ($\lambda = 25$). The experimental results are reported in Table 3. It is evident that our method yields higher PSNR and SSIM on both noises, and our method is much more stable (our method has $> 10\times$ lower standard deviation compared with *DM-DM*), suggesting that the benefits of our method are likely not due to over-parameterization.

4. CONCLUSION

In this paper, we propose a novel joint demosaicing and denoising method, dubbed *JDD-DoubleDIP*, which consists of a denoising DIP to explicitly account for noise removal and a demosaicing DIP for high-quality full-color RGB image generation. By training these two DIPs jointly, our method yields better PSNR, SSIM, and perceived visual quality on Kodak and McMaster datasets under different noise types and intensities compared to other methods. In the future, we would like to investigate the explicit incorporation of prior information from the green channel into our method to boost performance, as it has twice as much information as the red or blue channels in a RAW image.

References

- [1] Michaël Gharbi, Gaurav Chaurasia, Sylvain Paris, and Frédo Durand, “Deep joint demosaicking and denoising,” *ACM Trans. Graph.*, vol. 35, no. 6, pp. 191:1–191:12, 2016.
- [2] Lin Liu, Xu Jia, Jianzhuang Liu, and Qi Tian, “Joint demosaicking and denoising with self guidance,” in *2020 IEEE/CVF Conference on Computer Vision and Pattern Recognition, CVPR 2020, Seattle, WA, USA, June 13-19, 2020*. 2020, pp. 2237–2246, Computer Vision Foundation / IEEE.
- [3] Samuel W. Hasinoff, “Photon, poisson noise,” in *Computer Vision, A Reference Guide*, pp. 608–610. 2014.
- [4] Guocheng Qian, Yuanhao Wang, Jinjin Gu, Chao Dong, Wolfgang Heidrich, Bernard Ghanem, and Jimmy S. Ren, “Rethinking learning-based demosaicing, denoising, and super-resolution pipeline,” in *IEEE International Conference on Computational Photography, ICCP 2022, Pasadena, CA, USA, August 1-5, 2022*. 2022, pp. 1–12, IEEE.
- [5] Qiyu Jin, Gabriele Facciolo, and Jean-Michel Morel, “A review of an old dilemma: Demosaicking first, or denoising first?,” in *2020 IEEE/CVF Conference on Computer Vision and Pattern Recognition, CVPR Workshops 2020, Seattle, WA, USA, June 14-19, 2020*. 2020, pp. 2169–2179, Computer Vision Foundation / IEEE.
- [6] Keigo Hirakawa and Thomas W. Parks, “Joint demosaicking and denoising,” *IEEE Trans. Image Process.*, vol. 15, no. 8, pp. 2146–2157, 2006.
- [7] Laurent Condat and Saleh Mosaddegh, “Joint demosaicking and denoising by total variation minimization,” in *19th IEEE International Conference on Image Processing, ICIP 2012, Lake Buena Vista, Orlando, FL, USA, September 30 - October 3, 2012*. 2012, pp. 2781–2784, IEEE.
- [8] Felix Heide, Markus Steinberger, Yun-Ta Tsai, Mushfiqur Rouf, Dawid Pajak, Dikpal Reddy, Orazio Gallo, Jing Liu, Wolfgang Heidrich, Karen Egiazarian, Jan Kautz, and Kari Pulli, “FlexISP: a flexible camera image processing framework,” *ACM Transactions on Graphics*, vol. 33, no. 6, pp. 231:1–231:13, Nov. 2014.
- [9] Daniel Khashabi, Sebastian Nowozin, Jeremy Jancsary, and Andrew W. Fitzgibbon, “Joint demosaicking and denoising via learned nonparametric random fields,” *IEEE Trans. Image Process.*, vol. 23, no. 12, pp. 4968–4981, 2014.
- [10] Teresa Klatzer, Kerstin Hammernik, Patrick Knöbelreiter, and Thomas Pock, “Learning joint demosaicking and denoising based on sequential energy minimization,” in *2016 IEEE International Conference on Computational Photography, ICCP 2016, Evanston, IL, USA, May 13-15, 2016*. 2016, pp. 1–11, IEEE Computer Society.
- [11] Thibaud Ehret, Axel Davy, Pablo Arias, and Gabriele Facciolo, “Joint demosaicking and denoising by fine-tuning of bursts of raw images,” in *2019 IEEE/CVF International Conference on Computer Vision, ICCV 2019, Seoul, Korea (South), October 27 - November 2, 2019*. 2019, pp. 8867–8876, IEEE.
- [12] Yunjin Park, Sukho Lee, Byeongseon Jeong, and Jungho Yoon, “Joint demosaicking and denoising based on a variational deep image prior neural network,” *Sensors*, vol. 20, no. 10, pp. 2970, 2020.
- [13] Dmitry Ulyanov, Andrea Vedaldi, and Victor S. Lempitsky, “Deep image prior,” in *2018 IEEE Conference on Computer Vision and Pattern Recognition, CVPR 2018, Salt Lake City, UT, USA, June 18-22, 2018*. 2018, pp. 9446–9454, Computer Vision Foundation / IEEE Computer Society.
- [14] Taihui Li, Hengkang Wang, Zhong Zhuang, and Ju Sun, “Deep random projector: Accelerated deep image prior,” in *Proceedings of the IEEE/CVF Conference on Computer Vision and Pattern Recognition*, 2023, pp. 18176–18185.
- [15] Taihui Li, Zhong Zhuang, Hengkang Wang, and Ju Sun, “Random Projector: Efficient Deep Image Prior,” in *ICASSP 2023 - 2023 IEEE International Conference on Acoustics, Speech and Signal Processing (ICASSP)*, June 2023, pp. 1–5.
- [16] Yossi Gandelsman, Assaf Shocher, and Michal Irani, “double-dip”: Unsupervised image decomposition via coupled deep-image-priors,” in *IEEE Conference on Computer Vision and Pattern Recognition, CVPR 2019, Long Beach, CA, USA, June 16-20, 2019*. 2019, pp. 11026–11035, Computer Vision Foundation / IEEE.
- [17] Dongwei Ren, Kai Zhang, Qilong Wang, Qinghua Hu, and Wangmeng Zuo, “Neural blind deconvolution using deep priors,” in *2020 IEEE/CVF Conference on Computer Vision and Pattern Recognition, CVPR 2020, Seattle, WA, USA, June 13-19, 2020*. 2020, pp. 3338–3347, Computer Vision Foundation / IEEE.
- [18] Zhong Zhuang, Taihui Li, Hengkang Wang, and Ju Sun, “Blind Image Deblurring with Unknown Kernel Size and Substantial Noise,” *International Journal of Computer Vision*, Sept. 2023.
- [19] Sriram Ravula and Alexandros G. Dimakis, “One-dimensional deep image prior for time series inverse problems,” in *56th Asilomar Conference on Signals, Systems, and Computers, ASSC 2022, Pacific Grove, CA, USA, October 31 - Nov. 2, 2022*. 2022, pp. 1005–1009, IEEE.
- [20] Taihui Li, Zhong Zhuang, Hengyue Liang, Le Peng, Hengkang Wang, and Ju Sun, “Self-validation: Early stopping for single-instance deep generative priors,” in *32nd British Machine Vision Conference 2021, BMVC 2021, Online, November 22-25, 2021*. 2021, p. 108, BMVA Press.
- [21] “Kodak lossless true color image suite,” <https://r0k.us/graphics/kodak/>.
- [22] Lei Zhang, Xiaolin Wu, Antoni Buades, and Xin Li, “Color demosaicking by local directional interpolation and nonlocal adaptive thresholding,” *J. Electronic Imaging*, vol. 20, no. 2, pp. 023016, 2011.
- [23] Diederik P. Kingma and Jimmy Ba, “Adam: A method for stochastic optimization,” in *3rd International Conference on Learning Representations, ICLR 2015, San Diego, CA, USA, May 7-9, 2015, Conference Track Proceedings*, Yoshua Bengio and Yann LeCun, Eds., 2015.